Reducing the Biases in Simulated Radar Reflectivities from a Bulk Microphysics Scheme: Tropical Convective Systems

STEPHEN E. LANG

Laboratory for Atmospheres, NASA Goddard Space Flight Center, Greenbelt, and Science Systems and Applications, Inc., Lanham, Maryland

WEI-KUO TAO

Laboratory for Atmospheres, NASA Goddard Space Flight Center, Greenbelt, Maryland

XIPING ZENG

Laboratory for Atmospheres, NASA Goddard Space Flight Center, Greenbelt, and Goddard Earth Sciences and Technology Center, University of Maryland, Baltimore County, Baltimore, Maryland

YAPING LI

IMSG, NOAA/NESDIS/STAR, Camp Springs, Maryland

(Manuscript received 12 November 2010, in final form 3 March 2011)

ABSTRACT

A well-known bias common to many bulk microphysics schemes currently being used in cloud-resolving models is the tendency to produce excessively large reflectivity values (e.g., 40 dBZ) in the middle and upper troposphere in simulated convective systems. The Rutledge and Hobbs–based bulk microphysics scheme in the Goddard Cumulus Ensemble model is modified to reduce this bias and improve realistic aspects. Modifications include lowering the efficiencies for snow/graupel riming and snow accreting cloud ice; converting less rimed snow to graupel; allowing snow/graupel sublimation; adding rime splintering, immersion freezing, and contact nucleation; replacing the Fletcher formulation for activated ice nuclei with that of Meyers et al.; allowing for ice supersaturation in the saturation adjustment; accounting for ambient RH in the growth of cloud ice to snow; and adding/accounting for cloud ice fall speeds. In addition, size-mapping schemes for snow/graupel were added as functions of temperature and mixing ratio, lowering particle sizes at colder temperatures but allowing larger particles near the melting level and at higher mixing ratios. The modifications were applied to a weakly organized continental case and an oceanic mesoscale convective system (MCS). Strong echoes in the middle and upper troposphere were reduced in both cases. Peak reflectivities agreed well with radar for the weaker land case but, despite improvement, remained too high for the MCS. Reflectivity distributions versus height were much improved versus radar for the less organized land case but not for the MCS despite fewer excessively strong echoes aloft due to a bias toward weaker echoes at storm top.

1. Introduction

There has been a renewed interest recently in the parameterization and treatment of cloud microphysics in numerical models. Much of it has to do with continuing advances in computing power. Such advances have made it possible to incorporate (via nesting) cloud microphysics packages that were once reserved for cloud-scale models [i.e., cloud-resolving models (CRMs)] into mesoscale or regional-scale models such as the Weather Research and Forecasting model (WRF; Michalakes et al. 2004; Skamarock et al. 2008; http://www.wrf-model.org/index.php). Computing advances have also made it possible to employ much more sophisticated microphysics packages that require additional arrays (memory) and computations over reasonably large 3D domains and/or at reasonably fine resolution (~1–2 km or less). Despite

Corresponding author address: Stephen Lang, Mesoscale Atmospheric Processes Branch, Code 613.1, NASA GSFC, Greenbelt, MD 20771.
E-mail: stephen.e.lang@nasa.gov

DOI: 10.1175/JAS-D-10-05000.1

© 2011 American Meteorological Society

all of these advances, however, one-moment bulk microphysical schemes that have been around for 30 yr are still a valuable component in the numerical simulation and study of cloud systems because they are computationally more efficient than two-moment or multimoment schemes (e.g., Ferrier 1994; Morrison et al. 2005; Morrison and Grabowski 2008) and far more efficient than bin schemes (e.g., Khain and Sednev 1996; Ovtchinnikov and Kogan 2000; Khain et al. 2000, 2004), allowing them to be run over progressively larger domains and at simultaneously finer resolutions sooner (with respect to available computing resources) than the multimoment or bin schemes [see Table 1 in Tao et al. (2011) for a list of modeling studies involving bulk microphysics schemes over the years]. In addition to mesoscale and regional-scale models and longer-term or larger-scale CRM simulations, bulk schemes are also well suited for application in a multiscale modeling framework (MMF, or superparameterization). Nonetheless, in order to better understand and represent cloud processes, it is important that these bulk schemes be made more accurate by reducing some of their well-known biases especially since simulated cloud characteristics, which are directly linked with simulated cloud processes, are often used as a proxy for real clouds to indirectly retrieve cloud processes remotely (e.g., Tao et al. 1990, 1993, 2000, 2001, 2011; Olson et al. 1999, 2006; Smith et al. 1994; Yang and Smith 1999a,b, 2000; Shige et al. 2004, 2007, 2008, 2009; Grecu et al. 2009).

A lot of bulk microphysics schemes can trace their origins to the Lin et al. (1983) and Rutledge and Hobbs (1983, 1984) three-class ice schemes that were developed in the early 1980s. The Goddard Cumulus Ensemble (GCE) model is a CRM that has been developed and used to study convective cloud systems at the National Aeronautics and Space Administration (NASA) Goddard Space Flight Center over the past 30 yr and is among the models that have utilized these schemes. In early studies that included ice microphysics, model evaluation did not specifically focus on the actual microphysics but rather on the overall model itself and its ability to replicate the basic observed cloud structure or organization such as a convective leading edge and a trailing stratiform region (e.g., Fovell and Ogura 1988; Tao and Simpson 1989; Tao et al. 1991; Redelsperger et al. 2000; and many others) and/or specific observed features such as propagation speed, cold pool intensity, etc. (e.g., Nicholls 1987; Caniaux et al. 1994; Trier et al. 1996; and many others). With longer-term simulations, the approach has typically been to evaluate models by comparing basic mean profiles (e.g., temperature or moisture) or integrated quantities (such as precipitable water, outgoing longwave radiation, relative humidity, and surface rainfall) with similar observed quantities or even limited cloud observations in a time series or mean sense (e.g., Xu and Randall 1996; Xu et al. 2002; Zeng et al. 2007). This type of approach can identify overall model biases but only for those types of quantities. Early attempts to evaluate the actual ice microphysics were fairly indirect. McCumber et al. (1991), for example, determined that the Rutledge and Hobbs scheme was better suited for simulating tropical convection than the Lin scheme based mainly on the fact that it produced a higher stratiform percentage and larger simulated rain area at the surface and a better radar bright band. In situ aircraft data provide another much more direct means for assessing the microphysics (e.g., Murakami 1990; Brown and Swann 1997); however, although highly detailed, they do have a small sample volume and proper matching in space and time with equivalent model properties contains uncertainties.[1] It was the satellite retrieval community that first noticed a systematic bias in model-simulated ice contents. Using CRM-simulated cloud fields together with radiative transfer models to perform satellite retrievals, they found that the CRM scattering signatures were excessive and not well representative of actual observed distributions (Panegrossi et al. 1998; Bauer 2001; Olson et al. 2006), an indication that the models were producing excessive amounts of large precipitation-sized ice particles.

A number of more recent studies have begun to evaluate and/or improve CRM simulations (namely their microphysics) by comparing them against remote sensing data using statistical approaches, most notably contoured frequency with altitude diagrams (CFADs; Yuter and Houze 1995) or a variation there of (e.g., Eitzen and Xu 2005; Lang et al. 2007; Blossey et al. 2007; Zhou et al. 2007; Li et al. 2008; Matsui et al. 2009). These studies have invariably confirmed a bias in the simulations, namely an overabundance of stronger reflectivities aloft due to excessive precipitation-sized ice. Because simulated radar reflectivities or brightness temperatures are not unique solutions, these biases could be due to excessive graupel and/or snow amounts and/or sizes and/or densities. The objective of this study is built upon the improvements made to the GCE's bulk microphysics scheme in Lang et al. (2007) by further improving the model's synthetic radar reflectivity probability distributions (i.e., CFADs) in conjunction with reducing the bias in the overly deep penetration of strong reflectivities to upper levels. Climatologically, Zipser et al. (2006) showed that 40-dBZ

[1] Assuming the larger-scale flow features are properly represented, in situ and surface precipitation data can be valuable for evaluating microphysics schemes in mesoscale models especially in orographic studies where spatial features are strongly tied to the terrain (e.g., Colle and Mass 2000; Garvert et al. 2005; Colle et al. 2005).

echoes rarely penetrate above 10 km, but in the original GCE scheme this can occur even for moderately intense convection. The paper is organized as follows. In section 2, the model, the improvements to the microphysics and two case studies are described. In section 3, the results of the numerical experiments are compared against radar observations, and the summary and conclusions are given in section 4.

2. Numerical experiments

a. GCE model

The 3D GCE model will be used to evaluate the modifications made to the bulk microphysics scheme. Its main features are described in Tao and Simpson (1993) and Tao et al. (2003). The model has a 1.5-order subgrid-scale turbulence scheme (Soong and Ogura 1980) and parameterizations for shortwave (Chou and Suarez 1999), longwave (Chou and Kouvaris 1991; Chou et al. 1995, 1999; Kratz et al. 1998), and cloud optical properties (Sui et al. 1998; Fu and Liou 1993). In this study, the model will utilize positive definite advection (Smolarkiewicz 1983, 1984; Smolarkiewicz and Grabowski 1990), compressible flow (Klemp and Wilhelmson 1978), and the Rutledge and Hobbs (1983, 1984)–based three–ice class bulk microphysics scheme. The scheme has five prognostic hydrometeor variables (i.e., cloud water, rainwater, cloud ice, snow, and graupel) and was recently modified by Lang et al. (2007) to reduce the unrealistically large amount of precipitating ice particles (mainly graupel) and by Zeng et al. (2008, 2009) to introduce ice nuclei concentration into the parameterization for the Bergeron process.

b. Microphysics improvements

After the study by Lang et al. (2007), it was apparent that the bulk scheme required further modification, as there was still a noticeable bias in the simulated reflectivity distributions aloft with excessive probabilities at higher reflectivity values and peak values that were too strong. The bulk scheme was therefore systematically examined with each individual ice process reevaluated in light of the aforementioned biases and the assumption that the overall scheme was producing either too much and/or graupel that was too large and possibly likewise for snow. Some logical improvements were made as well. As a result, the following changes to the scheme were adopted. First, in addition to not allowing dry growth[2] following Lang et al. (2007), graupel amounts were directly reduced by effectively lowering the overall riming efficiency, tightening the thresholds for converting rimed snow to graupel, and allowing graupel to sublimate outside of cloud, which was not allowed in the original formulation. As cloud is assumed to be monodisperse (i.e., having a constant diameter of 20 μm), the graupel riming efficiency was made a function just of graupel size, with smaller sizes being less efficient and larger sizes more efficient (e.g., Khain et al. 2001). The riming thresholds for converting snow into graupel are fairly arbitrary but can have a large impact on graupel production (Rutledge and Hobbs 1984; Morrison and Grabowski 2008); however, based on comparisons with satellite and radar data (e.g., Lang et al. 2007), the scheme is almost certainly producing too much graupel. The thresholds were therefore adjusted to reduce the amount of graupel, which resulted in more snow.

Graupel amounts were also reduced indirectly by reducing the amount of supercooled cloud water available for riming. The original scheme lacked sufficient means to realistically convert cloud water to cloud ice in the mixed-phase region and relied on somewhat ad hoc settings in the saturation adjustment scheme to compensate. Outside of riming, the original scheme did not have the means to convert appreciable amounts of cloud liquid water to ice by the time air parcel temperatures fell to between $-12°$ and $-18°$C, at which very little liquid water is typically observed (e.g., Stith et al. 2002). To remedy this, three new processes were added: rime splintering, immersion freezing, and contact nucleation. In addition, the original Fletcher (1962) curve for the number of activated ice nuclei was replaced with the Meyers et al. (1992) formulation throughout the code. In conjunction with these changes, the sequential saturation scheme was relaxed. Water saturation, which is calculated first, was allowed to occur down to much colder temperatures followed by ice saturation, which was allowed to be supersaturated as is commonly observed (Jensen et al. 2001; Stith et al. 2002).

Preliminary testing showed that these changes alone were not enough to effectively reduce excessive simulated reflectivities at upper levels, so in addition to reducing the amount of graupel, a size-mapping scheme was introduced whereby the characteristic size (i.e., inverse of the slope parameter) of the inverse exponential graupel distribution was specified based on temperature and graupel mixing ratio, effectively lowering the size of graupel particles at colder temperatures while still allowing particles to be large near the melting level and at higher mixing ratios (see Fig. 1).[3]

[2] Dry growth may not be absolutely zero but should be quite small. Efficiencies are commonly set to very small values.

[3] Previous studies have varied the snow/graupel intercept as a function of either mixing ratio (Swann 1998; Reisner et al. 1998; Thompson et al. 2004) or temperature (Thompson et al. 2004; Hong et al. 2004).

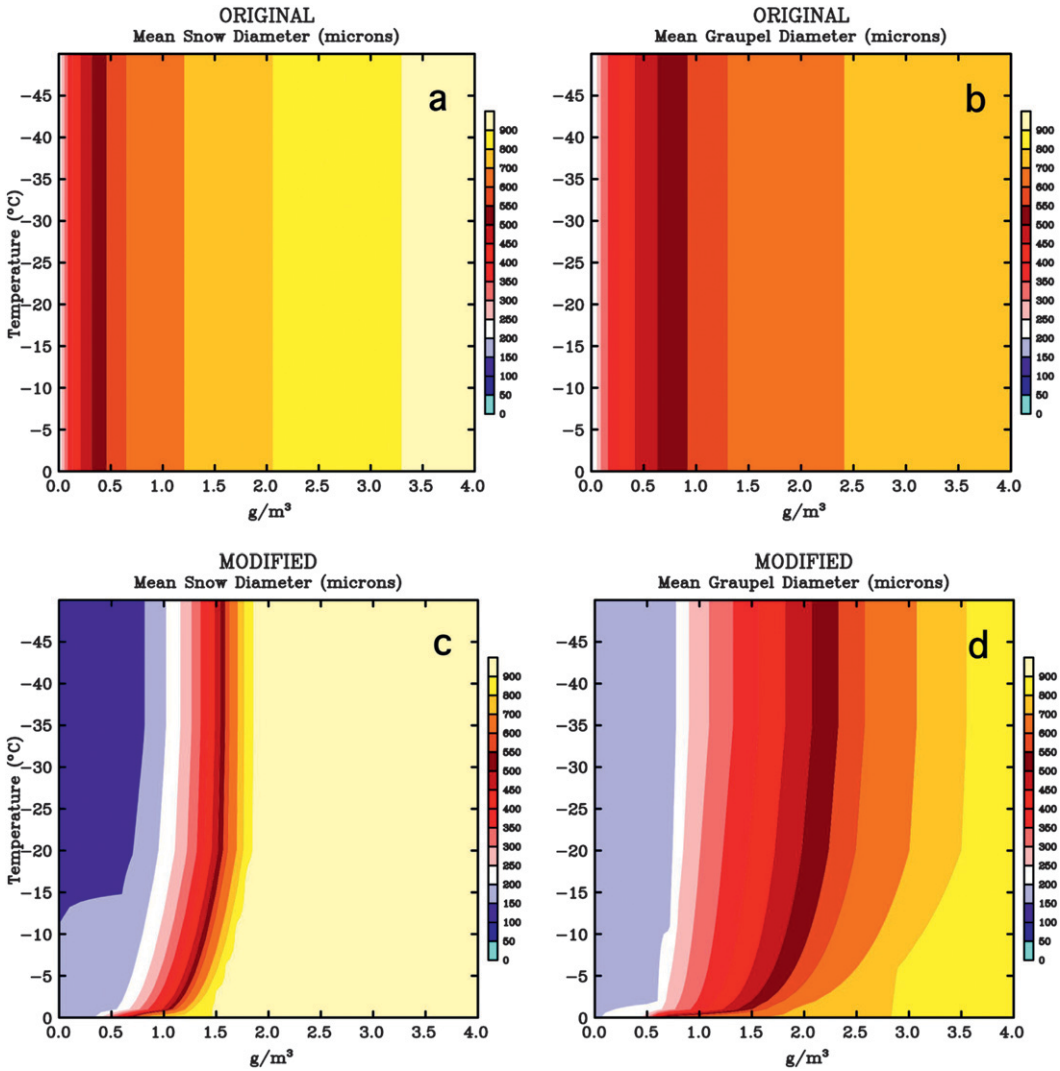

FIG. 1. Characteristic sizes (inverse of the slope parameter) of precipitation ice particle distributions (inverse exponential) as a function of precipitation ice content and temperature for (a) snow in the original Goddard scheme, which is based largely on Rutledge and Hobbs (1983, 1984), (b) graupel in the original Goddard scheme, (c) snow in the modified Goddard scheme, and (d) graupel in the modified Goddard scheme.

In addition to these changes to graupel, similar changes were required for snow to bring the core reflectivity probabilities more in line with observations. Snow amounts were reduced by effectively lowering the overall collection efficiency of cloud ice by snow (by again making the efficiency dependent on collector particle size with smaller sizes having a very low efficiency and larger sizes a moderate efficiency), allowing snow to sublimate outside of cloud (not allowed in the original formulation), and accounting for the ambient relative humidity and size of the cloud ice particles in the Bergeron process (i.e., Psfi) where cloud ice crystals grow into snow. In the original formulation for Psfi, the ambient relative humidity is implicitly assumed to be 100% with respect to water, which is often incorrect. This omission has been previously noted (e.g., Krueger et al. 1995). As with graupel, the characteristic sizes for snow were also mapped according to temperature and mixing ratio (Fig. 1), with small sizes at colder temperatures and low mixing ratios and larger sizes near the melting level and at higher mixing ratios. In addition to these changes, cloud ice fall speeds were added and accounted for in the sweep volume of those processes involving the accretion of cloud ice. Finally, the threshold for cloud ice autoconversion to snow was changed to physical units. Table 1 gives a summary of all of the changes along with more details.

TABLE 1. Microphysical processes modified or added to the original GCE Rutledge and Hobbs–based bulk microphysics scheme. Herein "$f(\cdot)$" indicates "function of." Also, Esi, Egc, and Esc are the collection efficiencies of cloud ice by snow, cloud by graupel, and cloud by snow, respectively; Qc0 is the cloud water mixing ratio; SSI, the supersaturation percentage with respect to ice; RH, the relative humidity; Vs/g, the snow/graupel fall velocity; Bh,i, the immersion mode ice nucleating efficiency; and Tair, the air temperature. The process nomenclature in the left column essentially follows Lin et al. (1983) and Rutledge and Hobbs (1983, 1984). Also, Dgacs and Dgaci are the graupel collection of snow and cloud ice for the dry mode, respectively, and Dgacw the graupel collection of cloud at temperatures below freezing.

Process	Original	Modified	Reference(s) and notes
Psaut	Efficiency f(Tair)	Efficiency fixed, threshold changed from g g^{-1} to g m^{-3}	—
Psaci	Esi = 0.1	Esi is f(snow diameter), maximum Esi = 0.25	See snow size mapping in Fig. 1
Praci	—	Accounts for addition of cloud ice fall speed	Cloud ice fall speed follows Hong et al. (2004)
Psfi	Independent of RH	Depends on RH, accounts for cloud ice size via Meyers, which depends on SSI	Meyers et al. (1992); Krueger et al. (1995)
Dgacs/Dgaci	—	Turned off	See Lang et al. (2007)
Dgacw	Egc = 1.0	Egc is f(graupel diameter), maximum Egc = 0.65	See graupel size mapping in Fig. 1; Khain et al. (2001)
Psacw/Pwacs	Esc = 1.0, Qc0 = 0.5 g kg^{-1}	Esc = 0.45, Qc0 = 1.0 g kg^{-1}	Lang et al. (2007); Morrison and Grabowski (2008)
Rime splintering	None	Added and applied to Psacw/Pgacw, not f(Vs/g) or f(cloud size)	Hallet and Mossop (1974); f(Tair) and splinter mass follow Ferrier (1994)
Pidw/Pidep	Based on Fletcher	Based on Meyers, which depends on SSI	Fletcher (1962); Meyers et al. (1992)
Pint	Based on Fletcher	Based on Meyers, which depends on SSI, previous ice concentration checked	Fletcher (1962); Meyers et al. (1992)
Immersion freezing	None	Added based on Diehl	Diehl and Wurzler (2004); Diehl et al. (2006), assumes Bh, I = 1.01×10^{-2} for pollen
Contact nucleation	None	Added based on Cotton and Pruppacher for Brownian diffusion only	Cotton et al. (1986); Pruppacher and Klett (1980), 500 active nuclei per cubic centimeter with radii of 0.1 μm
Saturation adjustment	Sequential based on Tao	Modified sequential, iterative, allows for SSI of up to 10%	Tao et al. (2003)
Snow/graupel Sublimation	None	Allowed if outside cloud and air subsaturated	—
Snow/graupel size	Based on fixed intercepts	Based on intercepts mapped according to snow/graupel mass and temperature	—
Cloud ice fall speed	None or based on Starr and Cox	Based on Hong	Hong et al. (2004); Starr and Cox (1985)

c. *Case studies*

1) A CONTINENTAL CONVECTIVE CASE: TRMM LBA

The 23 February 1999 case was one of the cases presented in Lang et al. (2007) and was characteristic of the westerly-regime type of convection observed during the Tropical Rainfall Measuring Mission (TRMM) Large-Scale Biosphere–Atmosphere Experiment in Amazonia (LBA) whereby convection was widespread, rather weak, and almost oceanic or monsoon-like in nature (Cifelli et al. 2002; Rickenbach et al. 2002). It was also a good case for diurnal growth and was used as such in a model intercomparison study by Grabowski et al. (2006). On this day, convection began in the late morning and because of the weak environmental winds became only weakly organized by early afternoon into southeast–northwest transient lines parallel to the deep tropospheric shear vector before dying out by evening. Please see Lang et al. (2007) for additional details. The model setup for this study also follows that used in Lang et al. (2007) with the same horizontally homogenous initial conditions based on morning sounding data, cyclic lateral boundary conditions, and convection initiated by

imposing time-varying (diurnal) surface fluxes based on surface observations collected at two different sites. The horizontal grid resolution was also kept at the same constant 250 m in both the x and y directions; however, in this study, the horizontal domain was expanded from 64×64 to 128×128 km^2 to allow more room for a convective line to form. In conjunction with this, the 32×32 km^2 patch of differing surface fluxes used in the original study was stretched in the north–south direction to a rectangular patch of 20×56 km^2. Although the total depth of the vertical domain was kept about the same near 23 km, the number of stretched vertical levels was increased from 41 to 70, and the sponge layer at the top was relaxed. Finally, the time step was reduced from 4 to 3 s.

2) AN OCEANIC CONVECTIVE SYSTEM: KWAJEX

As with TRMM LBA, the Kwajalein Experiment (KWAJEX) was also a TRMM field campaign. It was conducted in and around Kwajalein Atoll in the Marshall Islands from July to September 1999 for the purposes of gathering data on and characterizing oceanic clouds and convection in support of the TRMM satellite mission (Yuter et al. 2005). Areal average rain rates, echo areas, and echo tops were observed to follow typical lognormal distributions. During KWAJEX, rain was observed almost daily in association with small-scale passing convection embedded within the easterly trade winds. This was punctuated by occasional larger-scale MCSs containing broad areas of stratiform rain. Only three MCSs were observed during KWAJEX. One of those occurred on 11–12 August in association with the interaction between a mixed Rossby gravity wave and a Kelvin wave (Sobel et al. 2004). This case was modeled by Li et al. (2008), who used it to show the simulated radar reflectivity bias in the University of Utah's 3D CRM's bulk microphysics scheme. This case will also be used to evaluate the bulk microphysics improvements in the 3D GCE. Zeng et al. (2008) used the same KWAJEX forcing data, which were obtained from a variational analysis approach (Zhang et al. 2001) and which Li et al. (2008) used in their study, to conduct longer-term simulations with the GCE model. Following Li et al. (2008), for this case the model will be run for only 72 h starting at 0000 UTC 11 August using 500-m horizontal grid spacing. However, the domain size in this study will be larger, 128×128 km^2 as opposed to 64×64 km^2, and the vertical grid will follow the LBA setup.

3. Simulation results and validation

a. LBA

To make a proper comparison against the radar observations, an appropriate data sample from the model is required. Lang et al. (2007) utilized data from the entire domain (64×64 km^2) and selected an appropriate time period from the model based on having convective fractions that were closest to those from the radar analyses. The mean convective fraction for the radar observations is on the order of 0.4.[4] In this study, the use of the larger domain allowed the simulated convective line to become larger, more coherent, and longer in the north–south direction with the northern end having a more pronounced stratiform region. Therefore, in addition to a subperiod, a fixed subdomain was selected with the same size (i.e., 64×64 km^2) as the total domain used in the Lang et al. (2007) study to sample the northernmost portion of the transient line. Finally, as in Lang et al. (2007), the model data were averaged to the same resolution as the radar analyses (i.e., 1 km). The resulting mean convective fraction for the model using the improved microphysics over the subdomain for the subperiod 300–360 min is 0.47, a closer match than was obtained in the previous Lang et al. (2007) study. Figure 2 shows time–height cross sections of maximum reflectivity simulated from both the model[5] using the new microphysics modifications and the original scheme as well as the observations. In the original scheme, 40-dBZ echoes penetrate to over 13 km, and although perhaps at a stage when convection was less vigorous, ground-based radar observations show 40-dBZ echoes only reaching to 7 km. These excessive peak reflectivities in the original scheme are all due to graupel (see Fig. 4a) whereby excessive amounts in connection with a fixed intercept lead to large graupel sizes at higher altitudes and result in a major bias in peak reflectivities aloft (Fig. 2d). In contrast, the results from the modified physics show 40-dBZ echo penetrations that are greatly reduced, reaching to only 9 km. Peak reflectivity profiles taken from the final 60 min of the model runs, when the convective fractions better match the radar, show almost no bias in peak reflectivities for the modified physics.

Besides the improvement in the peak values, the modified scheme also results in a better overall reflectivity distribution. Figure 3 shows CFADs of radar reflectivity for the modified scheme, the original scheme, and the observations. Below the melting level (around 4.9 km), peak probabilities for the radar observations lie

[4] As in Lang et al. (2007), to match the radar observations, convective fractions were computed based on Rickenbach and Rutledge (1998), a texture algorithm applied to radar reflectivity data that largely follows the Steiner et al. (1995) method.

[5] Simulated radar reflectivities were calculated from the model rain, snow, and graupel contents and assumed inverse exponential size distributions using the formulation of Smith et al. (1975) and Smith (1984).

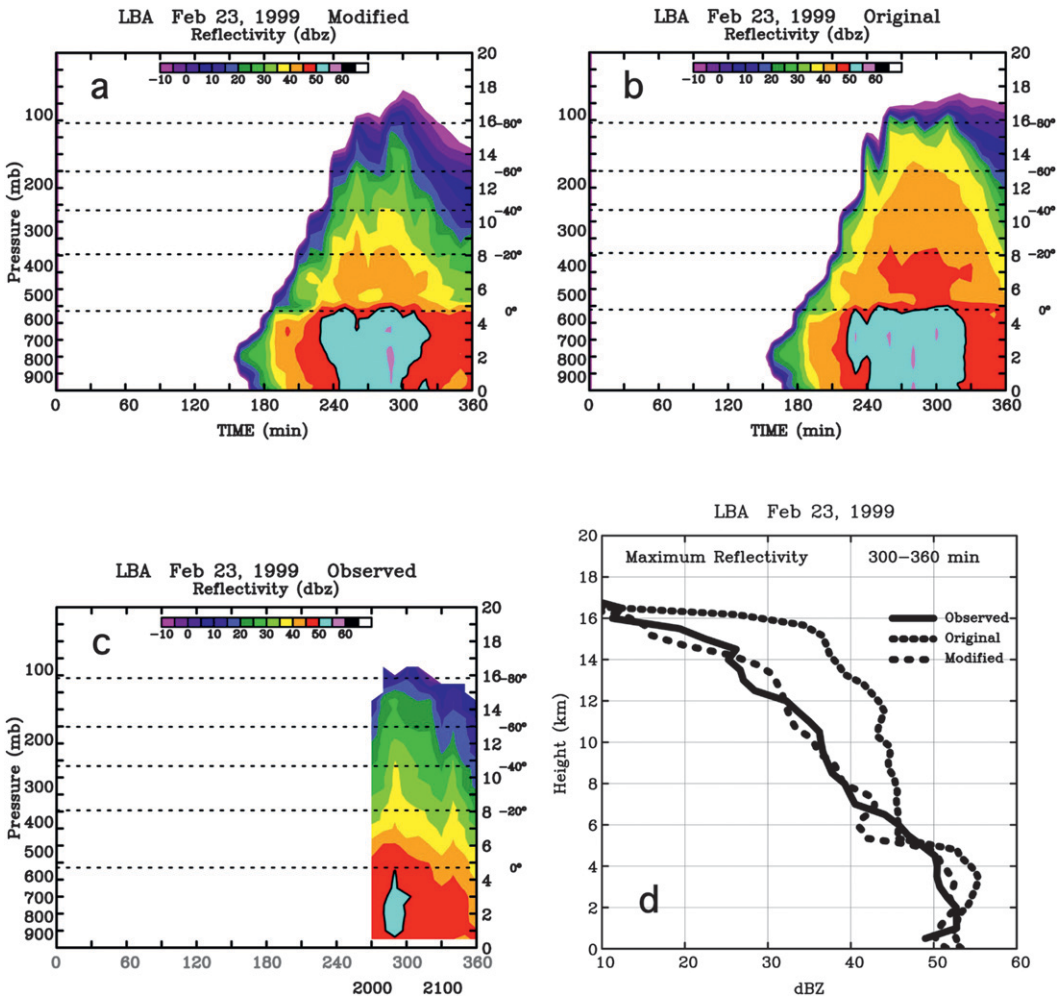

FIG. 2. Time–height cross sections of maximum radar reflectivity for the 23 Feb 1999 case simulated using (a) the modified Goddard microphysics scheme and (b) the original Goddard microphysics scheme, and observed by (c) ground-based radar and (d) vertical profiles of the maximum reflectivities extracted from the observations and the last 60 min of the simulations. Model data were taken from a 64 × 64 km^2 subdomain. Right axes in (a)–(c) are heights (km), horizontal dashed lines show the level of indicated environmental temperatures (°C). Black labels at the bottom of (c) are UTC times while gray labels indicate approximate matching model time.

between 5 and 15 dBZ, whereas they are shifted much higher, to between 25 and 40 dBZ, for the original scheme. And although there were no direct modifications made to the warm rain physics, the modified scheme does lead to noticeable improvement at lower levels with peak probabilities between 20 and 30 dBZ. Although significantly better than the original scheme, these still represent a significant bias and indicate that changes to the warm rain scheme or a size-mapping scheme for rain (e.g., Thompson et al. 2004) are needed. From the freezing level up to storm top near 16 km, the observed peak radar probabilities gradually diminish from between 5 and 20 dBZ to between about −5 and 15 dBZ (Fig. 3c). For the original scheme (Fig. 3b), peak probabilities are shifted significantly higher than the observed and range from approximately 20 to near 40 dBZ from the freezing level up to 9 km. It shows that the original scheme has a large bias of almost 20 dBZ in the vast majority of radar echoes in this region. In contrast, the CFAD for the modified scheme (Fig. 3a) shows a vast improvement over the original at midlevels, with excellent agreement between the observed and simulated peak probabilities from the melting level all the way up to 11 km. Above 9 km, the core of maximum probabilities for the original scheme falls off sharply but steadily down to between −10 and 5 dBZ at 16 km. The result is peak probabilities that are too strong up to 12 km, about right at 13–14 km, and too low at storm top. Within this region, there are also a number of echoes that are too strong and fall outside of the maxima of the observed distribution.

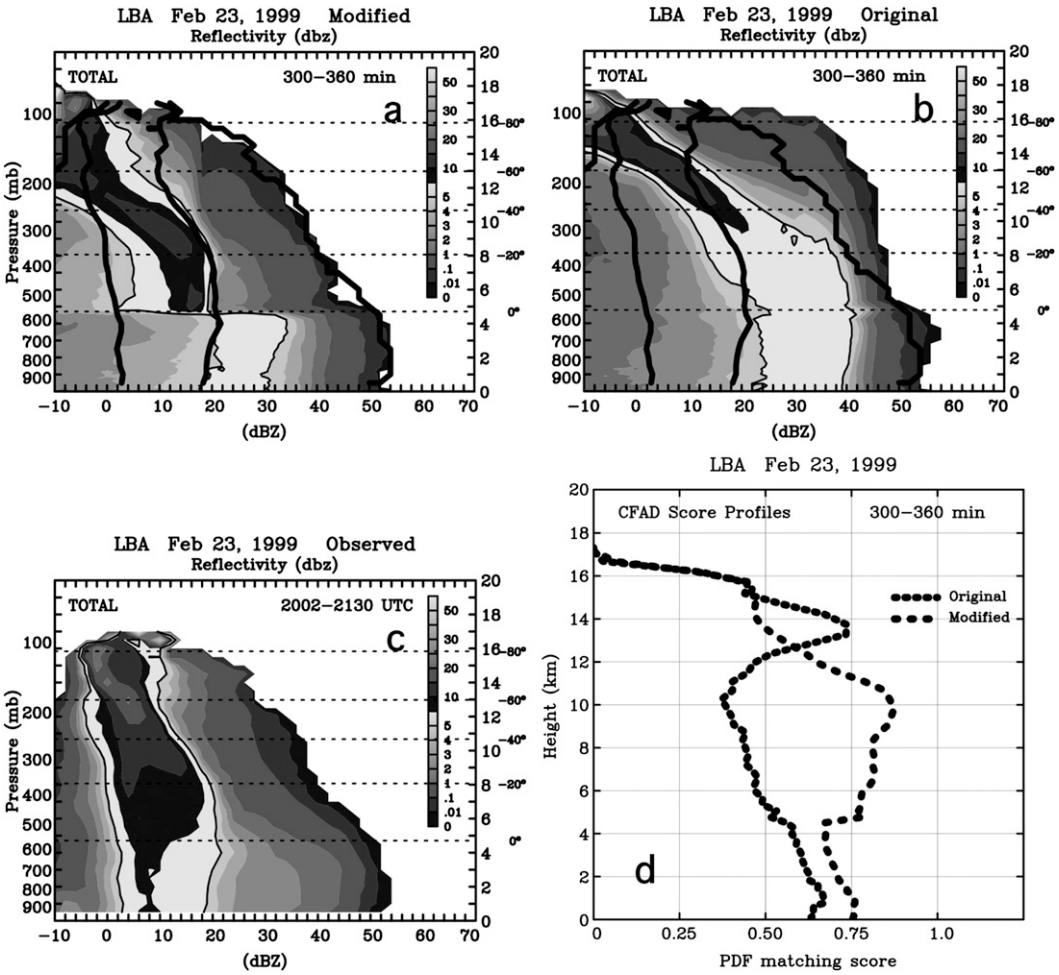

FIG. 3. Reflectivity CFADs for the 23 Feb 1999 case constructed from (a) the simulation using the modified Goddard microphysics scheme and (b) the simulation using the original Goddard microphysics scheme, together with (c) S-Pol ground-based radar observations and (d) vertical profiles of PDF matching scores (i.e., the PDF overlap at each level) between the observed and two simulated CFADs. Model data came from a 64×64 km^2 subdomain and the last 60 min of the simulations. The thick lines in (a) and (b) mark the edges of the core of the maximum observed probabilities [i.e., the 5% contours shown in (c)] and the outer limits of the observed distributions [i.e., the 0% contours also shown in (c)]. Right axes in (a)–(c) are heights (km); horizontal dashed lines show the level of indicated environmental temperatures (°C).

Above 12 km, probabilities for the modified scheme also drop off too much and are skewed toward echoes that are too weak compared to the radar observations. The net overall agreement between the observed and simulated radar distributions (Fig. 3d) is determined by normalizing the sum of the absolute differences in the probability distribution functions (PDFs) at each level (two identical distributions would score 1.0 for unity, while two distributions with no overlap would score 0). For the original scheme, the results show modest agreement with observations below the melting level with scores of around 0.6 while the modified scheme is slightly but consistently better with scores around 0.7. From the melting level up to 12 km, the original scheme does poorly with scores below 0.5, indicating there is more disagreement than agreement, whereas the modified scheme shows considerable improvement in this region with scores closer to 0.8. The original scheme has better overall agreement around 13–14 km; however, the modified scheme eliminates the excessively strong echoes present in the original scheme in this region. Above 14 km, both the original and modified schemes do poorly as both underestimate the echo intensities near storm top.

Mean hydrometeor profiles for the two schemes (Fig. 4) show that graupel is far and away the dominant species in the original scheme, as already noted by Lang et al. (2007). In contrast, in the modified scheme, snow is now comparable to graupel in the first 1–2 km above the

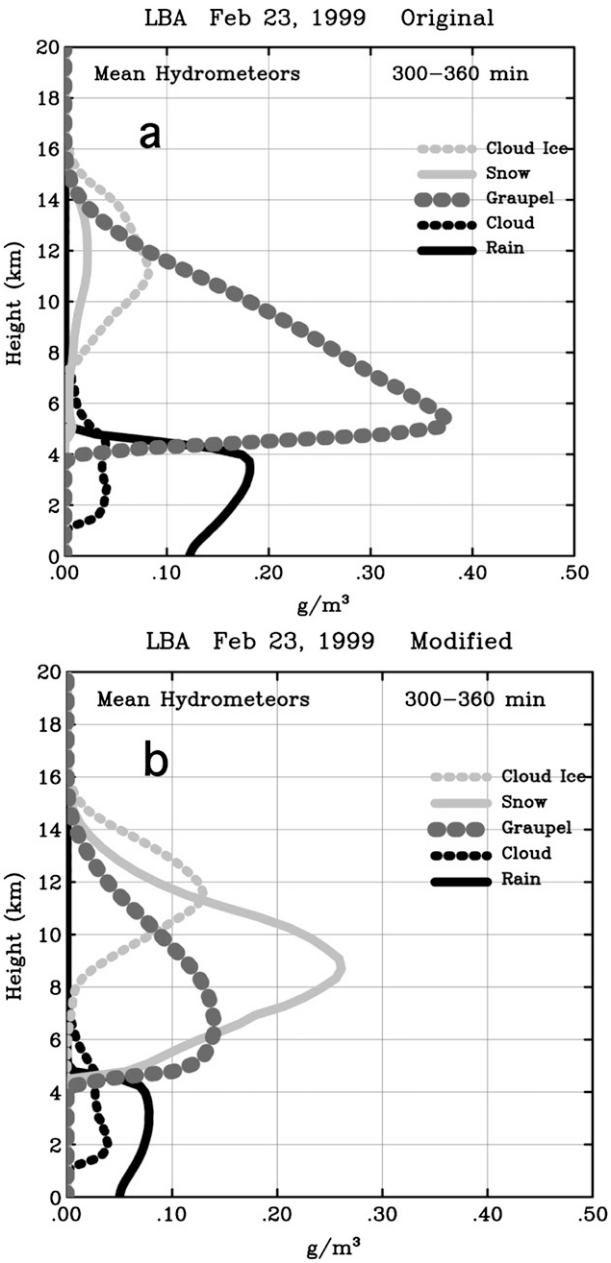

FIG. 4. Vertical profiles of domain and time-averaged hydrometeor species for the 23 Feb 1999 simulations using (a) the original Goddard microphysics scheme and (b) the modified Goddard microphysics scheme. Model data were taken from a 64×64 km^2 subdomain and the last 60 min of the simulations.

freezing level and is the dominant species at midlevels, while cloud ice is the largest at upper levels.

b. KWAJEX

Figure 5 shows time–height cross sections of maximum reflectivity for the 11–12 August 1999 KWAJEX case simulated by the model using the newly modified microphysics and the original scheme for the entire simulation period as well as the actual radar observations from when the system was in range of the radar. The original scheme has a large bias with 40-dBZ echoes frequently penetrating to between 12 and 14 km whereas the corresponding radar observations show 40-dBZ echoes only reaching to between 5 and 7 km. In contrast to the base scheme, the 40-dBZ echo penetrations in the modified scheme are noticeably reduced, ranging up to between 9 and 11 km. The high bias is significantly reduced but not eliminated. Peak reflectivity profiles taken from the radar and the corresponding period in the model runs show a high bias on the order of 10 dBZ for the original scheme in the middle and upper troposphere (from 7 to 14 km). This high bias is greatly reduced in the upper troposphere (above 10 km) in the modified scheme but not in the middle troposphere (from 6 to 10 km), where peak reflectivity values are nearly the same (Fig. 5d). There is a sharp dropoff, however, in peak reflectivity above 15 km in both schemes, resulting in an actual low bias in the simulated echo tops compared to the radar observations.

Reflectivity CFADs as well as profiles of the overlap between the observed and simulated PDFs at each level are shown in Fig. 6. Unlike the LBA case, the modified physics do not result in an overall substantial improvement in the radar reflectivity distribution. The simulated PDFs are consistently better below the melting layer but only slightly. Above the melting layer, the overall agreement between the new and old physics is essentially the same; however, the unsubstantiated occurrence of high reflectivities (e.g., 40 dBZ) in the upper troposphere is substantially reduced in the new physics, as was intended. This benefit is offset by a relative increase in the number of weak echoes from -10 to 0 dBZ such that the overall PDF score remains the same. This issue of having a disproportionately high amount of weak echoes is especially problematic at storm top as evidenced in both the LBA and KWAJEX results for both the modified and original physics. It causes the reflectivity PDFs to shift dramatically to weaker echoes between -10 and 0 dBZ whereas the radar data indicates the most common echoes at storm top are between -4 and 14 dBZ for LBA and between 8 and 18 dBZ for KWAJEX. The reasons for this bias are not altogether clear but could be due to entrainment effects. When drier air is entrained into the tops of convective towers, which have carried both smaller and larger ice particles aloft, it could disproportionately affect smaller particles by causing them to sublimate more as a result of their larger relative surface area and thereby cause the characteristic particle size to be relatively large. The observed KWAJEX CFAD shows peak probabilities actually increasing with height

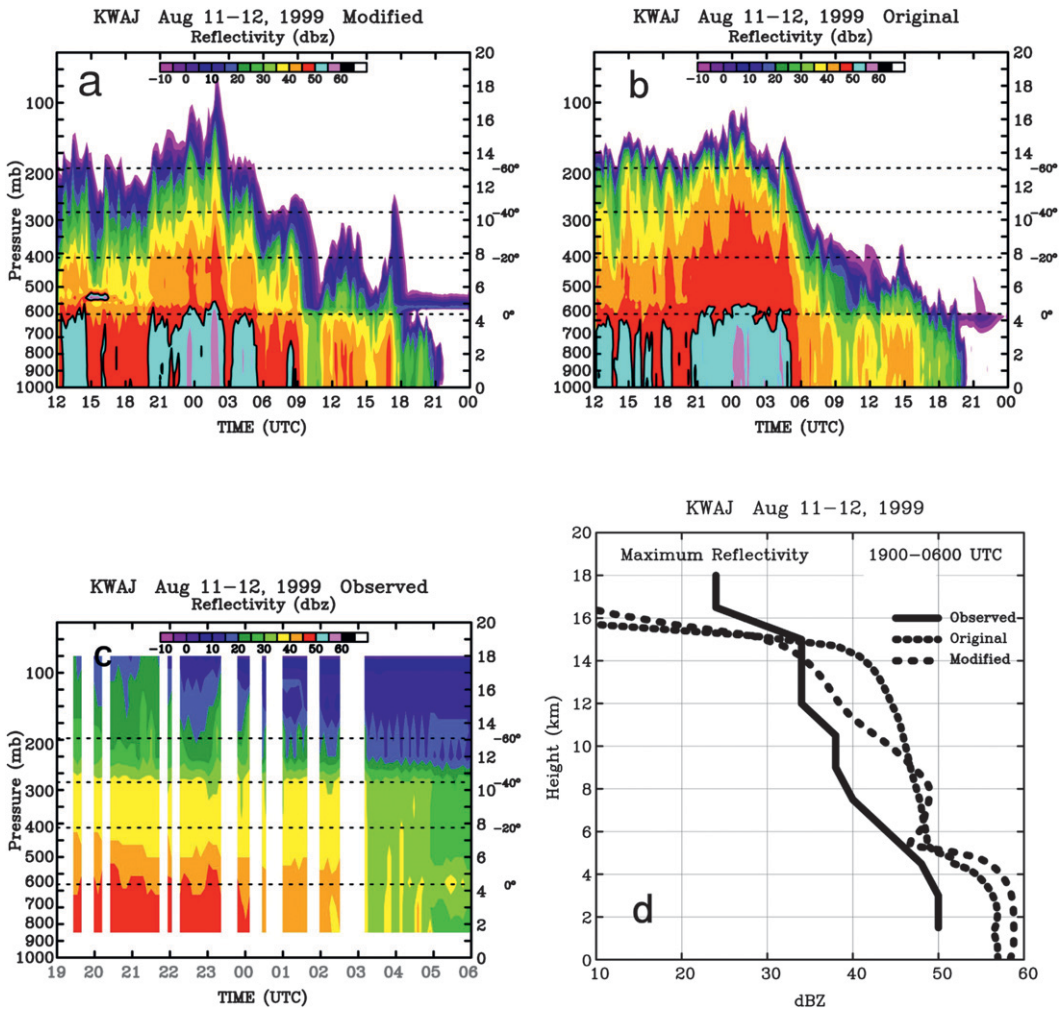

FIG. 5. Time–height cross sections of maximum radar reflectivity for the 11–12 Aug 1999 case simulated using (a) the modified Goddard microphysics scheme and (b) the original Goddard microphysics scheme, and (c) observed by ground-based radar and (d) vertical profiles of the observed and simulated maximum reflectivities. Right axes in (a)–(c) are heights (km); horizontal dashed lines show the level of indicated environmental temperatures (°C).

to higher reflectivities. This means that even though snow or graupel mixing ratios are small, their particle sizes could be somewhat large, which poses a challenge for the size-mapping scheme. Luo et al. (2009) constructed normalized CFADs from *CloudSat* data for convective profiles and anvils and found rather distinct differences between the two regions. In the anvil region, peak probabilities near the top of the cloud were maximized at the lowest reflectivities and spread to higher values lower down in the cloud, suggesting that particle sizes increased from small to larger with decreasing altitude through accretion and aggregation whereas the spectrum of particle sizes was broader in the convective region and included a mixture of small and larger particles. The modeled CFADs (both the original and modified) appear similar to the *CloudSat* anvil distributions at upper levels because of the preponderance of small particles at cloud top as a result of the simulated distributions of snow and graupel content combined with the snow and graupel mapping schemes.

4. Summary and conclusions

The Rutledge and Hobbs–based three-class ice scheme (cloud ice, snow, and graupel) was modified to reduce the unrealistic penetration of high reflectivity values (e.g., 40 dBZ) into the middle and upper troposphere in simulations of tropical convective systems using the Goddard Cumulus Ensemble CRM. The modifications first entailed individual changes to the parameterizations of specific processes including the addition of three new processes not previously included as well as a particle

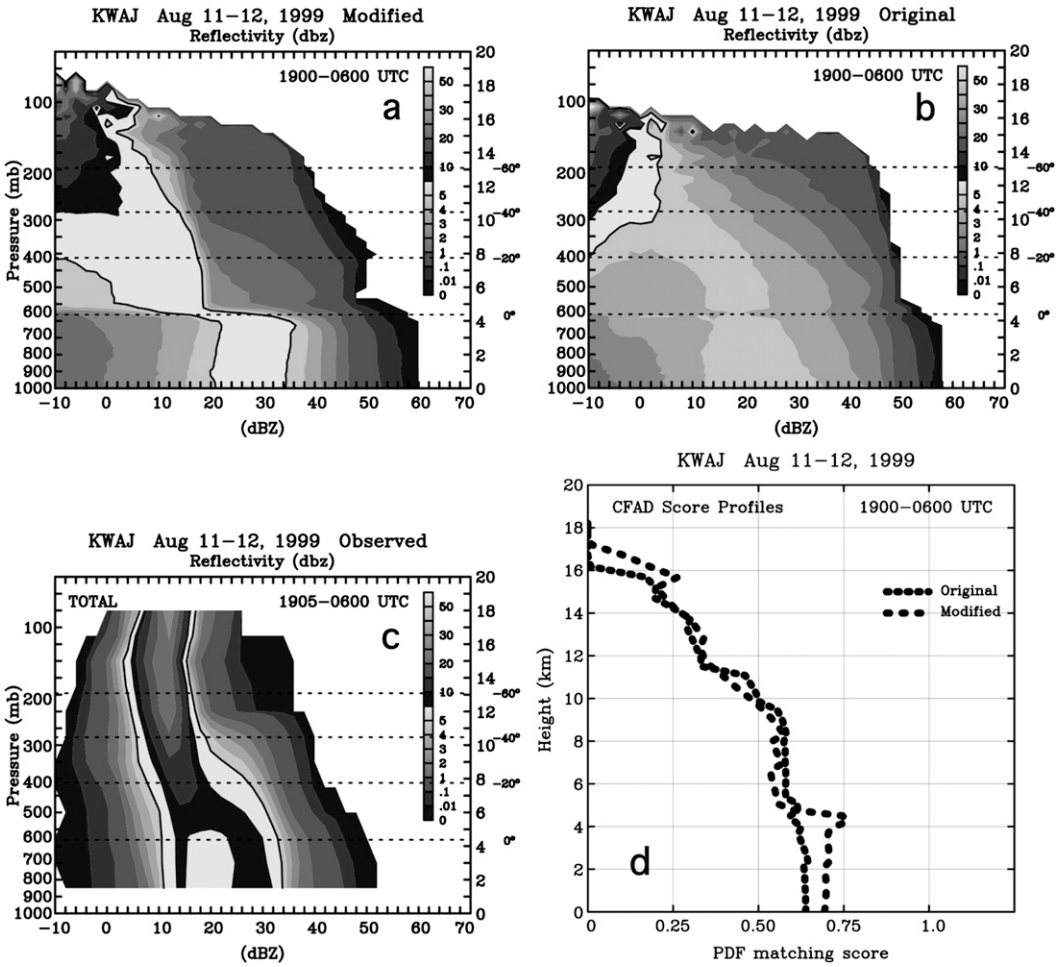

FIG. 6. Reflectivity CFADs for the 11–12 Aug 1999 case constructed from (a) the simulation using the modified Goddard microphysics scheme, (b) the simulation using the original Goddard microphysics scheme, and (c) Kwajalein ground-based radar observations, and (d) vertical profiles of PDF matching scores (i.e., the PDF overlap at each level) between the observed and two simulated CFADs. Right axes in (a)–(c) are heights (km), while horizontal dashed lines show the level of indicated environmental temperatures (°C).

size-mapping scheme for snow and graupel. Previous results (i.e., Lang et al. 2007) suggested that despite some improvements to the scheme, the bulk microphysics were still producing too much large precipitation-sized ice aloft. The latest modifications involved the reduction of the collection efficiencies of cloud ice by snow, cloud by graupel, and cloud by snow—the first two were made functions of the snow and graupel particle sizes, respectively. The cloud water threshold for generating graupel via snow riming was also increased. Three new parameterizations for rime splintering, immersion freezing, and contact nucleation were included to more realistically simulate the transition of cloud water to cloud ice. In conjunction, this allowed the saturation adjustment scheme to be relaxed to allow water saturation to colder temperatures and the presence of ice super saturation. The original Fletcher (1962) curve for the number of activated ice nuclei was replaced with the Meyers et al. (1992) formulation in the appropriate cloud ice–related processes (i.e., cloud ice initiation, deposition, and growth from cloud water). Cloud ice fall speeds based on Hong et al. (2004) were added and their effects on the appropriate sweep volumes included. Finally, several process were modified to be more logical or consistent—graupel and snow were allowed to sublimate outside of cloudy areas, the threshold for snow autoconversion was changed to physical units, and relative humidity and cloud ice particle size [via the Meyers et al. (1992) formulation] were accounted for in the growth of cloud ice particles to snow via the Bergeron process. In addition to these changes to specific processes, size mapping schemes for snow and graupel were

incorporated whereby the characteristic size (i.e., inverse of the slope parameter) of the inverse exponential snow or graupel distribution was specified based on temperature and snow or graupel mixing ratio, effectively lowering the size of snow and graupel particles at colder temperatures while still allowing particles to be large near the melting level and at higher mixing ratios.

These modifications were applied first to a weakly organized continental case observed during TRMM LBA and an oceanic MCS observed during KWAJEX. In both cases, the penetration of strong echoes (e.g., 40 dBZ) into the middle and upper troposphere was notably reduced. For LBA the agreement in maximum reflectivities with height with ground-based radar data was quite good. With KWAJEX, the modified bulk scheme still resulted in peak reflectivities that were too high in the middle troposphere, but the overall bias, especially in the upper troposphere, was significantly improved compared to the original scheme. Comparisons of reflectivity distributions yielded mixed results. For LBA, the new scheme improved the agreement with the radar PDFs below the melting level but especially over a 7-km deep layer at midlevels above the melting level; however, there was no improvement in the uppermost part of the storm. For KWAJEX, there was a significant reduction in the occurrence of excessively high reflectivities aloft, but there was almost no improvement in the overall agreement with the radar CFAD because of a worse bias in the preponderance of weak echoes. There was, however, minor improvement below the melting level. The new scheme resulted in a significant shift in the mean hydrometeor profiles. While graupel is far and away the dominant species in the original scheme, for the new scheme snow is comparable to graupel just above the freezing level and is the dominant species at midlevels while cloud ice is the most abundant species at upper levels.

Overall, the modifications to the scheme did significantly help to reduce the bias in the overabundance and excessive penetration of strong (e.g., 40 dBZ) echoes in the middle and upper troposphere in tropical convective cloud systems from two different environments. This should in turn improve the radar and satellite signatures of the simulated systems, making the simulated cloud datasets more valuable. The size-mapping scheme offers a partial yet economical workaround to having a single moment. The current mapping is somewhat of a first guess based largely upon inducing the model into producing a better reflectivity distribution and may require further revision but most likely should depend upon both temperature and mass. The fact that moderate reflectivity values (e.g., 30 dBZ) are regularly observed in the middle and upper troposphere suggests that the size-mapping scheme needs to allow for the possibility of moderate-sized particles at upper levels; a temperature-only dependency for the intercept or slope parameters may not be sufficient especially in the convective region. Aircraft observations could be used to verify and improve the mapping, but their limited sample may not be sufficient to verify all possible combinations of mixing ratio and temperature. The biggest challenge to the mapping is that there may be considerable variation in particle size for a given mixing ratio and temperature depending on the environment or cloud history. One example of this is the positive bias in the amount of weak echoes at storm top present in both the original and modified schemes. The distribution of particle sizes at the top of convective versus stratiform clouds could be quite different (i.e., for the same mixing ratio, particle sizes could be characteristically larger in the convective region). The original scheme does not have the ability to account for particle history nor does the proposed mapping approach. Nonetheless, despite the possible limitations, it offers a way to at least partially overcome the fixed intercepts in the original scheme without having to use two moments. While mapping was only applied to the snow and graupel species, a variable intercept for rain could also be invoked (e.g., Thompson et al. 2004). In addition, this same mapping approach could also be adopted to map the snow and graupel densities in conjunction with the sizes. Furthermore, given the fact that the modifications to the individual processes together with the snow/graupel size mapping were able to nearly eliminate the high reflectivity bias in the weaker LBA case but not the stronger KWAJEX MCS, this suggests that additional measures involving the particle fall speeds may be required to overcome the lofting of large graupel mixing ratios into the middle and upper troposphere in stronger cases. One possible solution would be to map the fall speed coefficients (especially those for graupel) in accordance with the densities, making the size, density, and fall speed coefficients consist with one another and increasing the sedimentation of larger mixing ratios. This also suggests that even higher-density hail would be required to obtain reasonable reflectivity CFADs for intense midlatitude convection.

The modified scheme needs to be tested in additional environments, as the dominant precipitation mechanisms can be quite different. A cold season case without the presence of graupel, for example, could help to identify biases in the snow-related processes. For more intense convective cases, especially where in situ data are hard to obtain, remote sensing data seem to remain the best means to evaluate the physics as was done here. Remote sensing data also offer a potentially large sample when looking for biases (Matsui et al. 2009). Despite the improvements to the scheme, it is still a single-moment bulk

scheme and therefore limited in its ability to resolve certain processes. Ultimately, a two-moment approach, based perhaps on the improved single-moment scheme, seems to be the best compromise between simple bulk and expensive bin schemes. Finally, model biases in the simulated hydrometeor fields are not necessarily all due to the microphysics parameterizations. The microphysics are closely intertwined with the dynamics. A variety of factors (e.g., grid configurations, convective initiation, turbulence parameterizations, etc.) can impact the dynamics. Biases in the dynamics can translate into the microphysics. There could also be biases in both that must be addressed.

Acknowledgments. This research was supported by the NASA Precipitation Measuring Mission (PMM) and the NASA Modeling, Analysis, and Prediction (MAP) Program. The authors are grateful to Drs. Ramesh Kakar, Don Anderson, and David B. Considine at NASA headquarters for their support of this research; to Drs. Andrew Heymsfield and Derek Posselt and Prof. J.-P. Chen for their useful suggestions; to Dr. Robert Cifelli for providing the LBA radar data; and to Dr. Jiundar Chern for carefully checking the code. Acknowledgment is also made to the NASA Goddard Space Flight Center and NASA Ames Research Center computing facilities and to Dr. Tsengdar Lee at NASA HQ for the computational resources used in this research. We would also like to thank three anonymous reviewers for their constructive comments that improved this paper.

REFERENCES

Bauer, P., 2001: Over-ocean rainfall retrieval from multisensor data of the Tropical Rainfall Measuring Mission. Part I: Design and evaluation of inversion databases. *J. Atmos. Oceanic Technol.,* **18,** 1315–1330.

Blossey, P. N., C. S. Bretherton, J. Cetrone, and M. Kharoutdinov, 2007: Cloud-resolving model simulations of KWAJEX: Model sensitivities and comparisons with satellite and radar observations. *J. Atmos. Sci.,* **64,** 1488–1508.

Brown, P. R., and H. A. Swann, 1997: Evaluation of key microphysical parameters in three-dimensional cloud-model simulations using aircraft and multiparameter radar data. *Quart. J. Roy. Meteor. Soc.,* **123,** 2245–2275.

Caniaux, G., J.-L. Redelsperger, and J.-P. Lafore, 1994: A numerical study of the stratiform region of a fast-moving squall line. Part I: General description and water and heat budgets. *J. Atmos. Sci.,* **51,** 2046–2074.

Chou, M.-D., and L. Kouvaris, 1991: Calculations of transmission functions in the IR CO_2 and O_3 bands. *J. Geophys. Res.,* **96,** 9003–9012.

——, and M. J. Suarez, 1999: A shortwave radiation parameterization for atmospheric studies. NASA Tech. Rep. NASA/TM-1999-10460, Vol. 15, 38 pp.

——, W. Ridgeway, and M.-H. Yan, 1995: Parameterizations for water vapor IR radiative transfer in both the middle and lower atmospheres. *J. Atmos. Sci.,* **52,** 1159–1167.

——, K.-T. Lee, S.-C. Tsay, and Q. Fu, 1999: Parameterization for cloud longwave scattering for use in atmospheric models. *J. Climate,* **12,** 159–169.

Cifelli, R., W. A. Petersen, L. D. Carey, S. A. Rutledge, and M. A. F. da Silva Dias, 2002: Radar observations of the kinematic, microphysical, and precipitation characteristics of two MCSs in TRMM LBA. *J. Geophys. Res.,* **107,** 8077, doi:10.1029/2000JD000264.

Colle, B. A., and C. F. Mass, 2000: The 5–9 February 1996 flooding event over the Pacific Northwest: Sensitivity studies and evaluation of the MM5 precipitation forecasts. *Mon. Wea. Rev.,* **128,** 593–617.

——, M. F. Garvert, J. B. Wolfe, C. F. Mass, and C. P. Woods, 2005: The 13–14 December 2001 IMPROVE-2 Event. Part III: Simulated microphysical budgets and sensitivity studies. *J. Atmos. Sci.,* **62,** 3535–3558.

Cotton, W. R., G. J. Tripoli, R. M. Rauber, and E. A. Mulvihill, 1986: Numerical simulation of the effects of varying ice crystal nucleation rates and aggregation processes on orographic snowfall. *J. Climate Appl. Meteor.,* **25,** 1658–1680.

Diehl, K., and S. Wurzler, 2004: Heterogeneous drop freezing in the immersion mode: Model calculations considering soluble and insoluble particles in the drops. *J. Atmos. Sci.,* **61,** 2063–2072.

——, M. Simmel, and S. Wurzler, 2006: Numerical sensitivity studies on the impact of aerosol properties and drop freezing modes on the glaciation, microphysics, and dynamics of clouds. *J. Geophys. Res.,* **111,** D07202, doi:10.1029/2005JD005884.

Eitzen, Z. A., and K.-M. Xu, 2005: A statistical comparison of deep convective cloud objects observed by an Earth Observing System satellite and simulated by a cloud-resolving model. *J. Geophys. Res.,* **110,** D15S14, doi:10.1029/2004JD005086.

Ferrier, B. S., 1994: A double-moment multiple-phase four-class bulk ice scheme. Part I: Description. *J. Atmos. Sci.,* **51,** 249–280.

Fletcher, N. H., 1962: *The Physics of Rain Clouds*. Cambridge University Press, 386 pp.

Fovell, R. G., and Y. Ogura, 1988: Numerical simulation of a midlatitude squall line in two dimensions. *J. Atmos. Sci.,* **45,** 3846–3879.

Fu, Q., and K.-N. Liou, 1993: Parameterization of the radiative properties of cirrus clouds. *J. Atmos. Sci.,* **50,** 2008–2025.

Garvert, M. F., C. P. Woods, B. A. Colle, C. F. Mass, P. V. Hobbs, M. T. Stoeligna, and J. B. Wolfe, 2005: The 13–14 December 2001 IMPROVE-2 event. Part II: Comparisons of MM5 model simulations of clouds and precipitation with observations. *J. Atmos. Sci.,* **62,** 3520–3534.

Grabowski, W. W., and Coauthors, 2006: Daytime convective development over land: A model intercomparison based on LBA observations. *Quart. J. Roy. Meteor. Soc.,* **132,** 317–344.

Grecu, M., W. S. Olson, C.-L. Shie, T. S. L'Ecuyer, and W.-K. Tao, 2009: Combining satellite microwave radiometer and radar observations to estimate atmospheric heating profiles. *J. Climate,* **22,** 6356–6376.

Hallet, J., and S. C. Mossop, 1974: Production of secondary ice particles during the riming process. *Nature,* **249,** 26–28.

Hong, S.-Y., J. Dudhia, and S.-H. Chen, 2004: A revised approach to ice microphysical processes for the bulk parameterization of clouds and precipitation. *Mon. Wea. Rev.,* **132,** 103–120.

Jensen, E., and Coauthors, 2001: Prevalence of ice supersaturated regions in the upper troposphere: Implications for optically thin ice cloud formation. *J. Geophys. Res.,* **106** (D15), 17 253–17 266.

Khain, A. P., and I. Sednev, 1996: Simulation of precipitation formation in the eastern Mediterranean coastal zone using a spectral microphysics cloud ensemble model. *Atmos. Res.,* **43,** 77–110.

——, M. Ovtchinnikov, M. Pinsky, A. Pokrovsky, and H. Krugliak, 2000: Notes on the state-of-the-art numerical modeling of cloud microphysics. *Atmos. Res.,* **55,** 159–224.

——, M. Pinsky, M. Shapiro, and A. Pokrovsky, 2001: Collision rate of small graupel and water drops. *J. Atmos. Sci.,* **58,** 2571–2595.

——, A. Pokrovsky, M. Pinsky, A. Seifert, and V. Phillips, 2004: Simulation of effects of atmospheric aerosols on deep turbulent convective clouds using a spectral microphysics mixed-phase cumulus cloud model. Part I: Model description and possible applications. *J. Atmos. Sci.,* **61,** 2963–2982.

Klemp, J. B., and R. B. Wilhelmson, 1978: The simulation of three-dimensional convective storm dynamics. *J. Atmos. Sci.,* **35,** 1070–1096.

Kratz, D. P., M.-D. Chou, M. M.-H. Yan, and C.-H. Ho, 1998: Minor trace gas radiative forcing calculations using the *k*-distribution method with one-parameter scaling. *J. Geophys. Res.,* **103,** 31 647–31 656.

Krueger, S. K., Q. A. Fu, K. N. Liou, and H. N. S. Chin, 1995: Improvements of an ice-phase microphysics parameterization for use in numerical simulations of tropical convection. *J. Appl. Meteor.,* **34,** 281–287.

Lang, S., W.-K. Tao, R. Cifelli, W. Olson, J. Halverson, S. Rutledge, and J. Simpson, 2007: Improving simulations of convective systems from TRMM LBA: Easterly and westerly regimes. *J. Atmos. Sci.,* **64,** 1141–1164.

Li, Y., E. J. Zipser, S. K. Krueger, and M. A. Zulauf, 2008: Cloud-resolving modeling of deep convection during KWAJEX. Part I: Comparison to TRMM satellite and ground-based radar observations. *Mon. Wea. Rev.,* **136,** 2699–2712.

Lin, Y.-L., R. D. Farley, and H. D. Orville, 1983: Bulk parameterization of the snow field in a cloud model. *J. Climate Appl. Meteor.,* **22,** 1065–1092.

Luo, Y., R. Zhang, and H. Wang, 2009: Comparing occurrences and vertical structures of hydrometeors between eastern China and the Indian monsoon region using *CloudSat*/CALIPSO data. *J. Climate,* **22,** 1052–1064.

Matsui, T., X. Zeng, W.-K. Tao, H. Masunaga, W. Olson, and S. Lang, 2009: Evaluation of long-term cloud-resolving model simulations using satellite radiance observations and multi-frequency satellite simulators. *J. Atmos. Oceanic Technol.,* **26,** 1261–1274.

McCumber, M., W.-K. Tao, J. Simpson, R. Penc, and S.-T. Soong, 1991: Comparison of ice-phase microphysical parameterization schemes using numerical simulations of tropical convection. *J. Appl. Meteor.,* **30,** 985–1004.

Meyers, M. P., P. J. DeMott, and W. R. Cotton, 1992: New primary ice-nucleation parameterizations in an explicit cloud model. *J. Appl. Meteor.,* **31,** 708–721.

Michalakes, J., J. Dudhia, D. Gill, T. Henderson, J. Klemp, W. Skamarock, and W. Wang, 2004: The Weather Research and Forecast model: Software architecture and performance. *Proc. 11th ECMWF Workshop on the Use of High Performance Computing in Meteorology,* Reading, UK, ECMWF, 156–168. [Available online at http://www.wrf-model.org/wrfadmin/docs/ecmwf_2004.pdf.]

Morrison, H., and W. W. Grabowski, 2008: A novel approach for representing ice microphysics in models: Description and tests using a kinematic framework. *J. Atmos. Sci.,* **65,** 1528–1548.

——, J. A. Curry, and V. I. Khvorostyanov, 2005: A new double-moment microphysics parameterization for application in cloud and climate models. Part I: Description. *J. Atmos. Sci.,* **62,** 1665–1677.

Murakami, M., 1990: Numerical modeling of dynamical and microphysical evolution of an isolated convective cloud—The 19 July 1981 CCOPE cloud. *J. Meteor. Soc. Japan,* **68,** 107–128.

Nicholls, M. E., 1987: A comparison of the results of a two-dimensional numerical simulation of a tropical squall line with observations. *Mon. Wea. Rev.,* **115,** 3055–3077.

Olson, W. S., C. D. Kummerow, Y. Hong, and W.-K. Tao, 1999: Atmospheric latent heating distributions in the tropics derived from passive microwave radiometer measurements. *J. Appl. Meteor.,* **38,** 633–664.

——, and Coauthors, 2006: Precipitation and latent heating distributions from satellite passive microwave radiometry. Part I: Method and uncertainties. *J. Appl. Meteor.,* **45,** 702–720.

Ovtchinnikov, M., and Y. L. Kogan, 2000: An investigation of ice production mechanisms in small cumuliform clouds using a 3D model with explicit microphysics. Part I: Model description. *J. Atmos. Sci.,* **57,** 2989–3003.

Panegrossi, G., and Coauthors, 1998: Use of cloud model microphysics for passive microwave-based precipitation retrieval: Significance of consistency between model and measurement manifolds. *J. Atmos. Sci.,* **55,** 1644–1673.

Pruppacher, H. R., and J. D. Klett, 1980: *Microphysics of Clouds and Precipitation*. D. Reidel, 714 pp.

Redelsperger, J. L., and Coauthors, 2000: A GCSS model intercomparison for a tropical squall line observed during TOGA-COARE. Part 1: Cloud-resolving models. *Quart. J. Roy. Meteor. Soc.,* **126,** 823–863.

Reisner, J., R. M. Rasmussen, and R. T. Bruintjes, 1998: Explicit forecasting of supercooled liquid water in winter storms using the MM5 mesoscale model. *Quart. J. Roy. Meteor. Soc.,* **124,** 1071–1107.

Rickenbach, T. M., and S. A. Rutledge, 1998: Convection in TOGA COARE: Horizontal scale, morphology, and rainfall production. *J. Atmos. Sci.,* **55,** 2715–2729.

——, R. N. Ferreira, J. B. Halverson, D. L. Herdies, and M. A. F. Silva Dias, 2002: Modulation of convection in the southwestern Amazon basin by extratropical stationary fronts. *J. Geophys. Res.,* **107,** 8040, doi:10.1029/2000JD000263.

Rutledge, S. A., and P. V. Hobbs, 1983: The mesoscale and microscale structure of organization of clouds and precipitation in midlatitude cyclones. VIII: A model for the "seeder-feeder" process in warm-frontal rainbands. *J. Atmos. Sci.,* **40,** 1185–1206.

——, and ——, 1984: The mesoscale and microscale structure and organization of clouds and precipitation in midlatitude cyclones. Part XII: A diagnostic modeling study of precipitation development in narrow cold-frontal rainbands. *J. Atmos. Sci.,* **41,** 2949–2972.

Shige, S., Y. N. Takayabu, W.-K. Tao, and D. E. Johnson, 2004: Spectral retrieval of latent heating profiles from TRMM PR data. Part I: Development of a model-based algorithm. *J. Appl. Meteor.,* **43,** 1095–1113.

——, ——, ——, and C.-L. Shie, 2007: Spectral retrieval of latent heating profiles from TRMM PR data. Part II: Algorithm improvement and heating estimates over tropical ocean regions. *J. Appl. Meteor. Climatol.,* **46,** 1098–1124.

——, ——, and ——, 2008: Spectral retrieval of latent heating profiles from TRMM PR data. Part III: Estimating apparent moisture sink profiles over tropical oceans. *J. Appl. Meteor. Climatol.,* **47,** 620–640.

——, ——, S. Kida, W.-K. Tao, X. Zeng, C. Yokoyama, and T. L'Ecuyer, 2009: Spectral retrieval of latent heating profiles from TRMM PR data. Part IV: Comparisons of lookup tables

from two- and three-dimensional cloud-resolving model simulations. *J. Climate,* **22,** 5577–5594.

Skamarock, W. C., and Coauthors, 2008: A description of the Advanced Research WRF Version 3. NCAR Tech. Note NCAR/TN-475+STR, 113 pp. [Available online at http://www.mmm.ucar.edu/wrf/users/docs/arw_v3.pdf.]

Smith, E. A., X. Xiang, A. Mugnai, and G. J. Tripoli, 1994: Design of an inversion-based precipitation profile retrieval algorithm using an explicit cloud model for initial guess microphysics. *Meteor. Atmos. Phys.,* **54,** 53–78.

Smith, P. L., 1984: Equivalent radar reflectivity factors for snow and ice particles. *J. Climate Appl. Meteor.,* **23,** 1258–1260.

——, C. G. Meyers, and H. D. Orville, 1975: Radar reflectivity factor calculations in numerical cloud models using bulk parameterization of precipitation. *J. Appl. Meteor.,* **14,** 1156–1165.

Smolarkiewicz, P. K., 1983: A simple positive definite advection scheme with small implicit diffusion. *Mon. Wea. Rev.,* **111,** 479–486.

——, 1984: A fully multidimensional positive definite advection transport algorithm with small implicit diffusion. *J. Comput. Phys.,* **54,** 325–362.

——, and W. W. Grabowski, 1990: The multidimensional positive advection transport algorithm: Nonoscillatory option. *J. Comput. Phys.,* **86,** 355–375.

Sobel, A. H., S. E. Yuter, C. S. Bretherton, and G. N. Kiladis, 2004: Large-scale meteorology and deep convection during TRMM KWAJEX. *Mon. Wea. Rev.,* **132,** 422–444.

Soong, S.-T., and Y. Ogura, 1980: Response of trade wind cumuli to large-scale processes. *J. Atmos. Sci.,* **37,** 2035–2050.

Starr, D., and S. K. Cox, 1985: Cirrus clouds. Part I: A cirrus cloud model. *J. Atmos. Sci.,* **42,** 2663–2681.

Steiner, M., R. A. Houze Jr., and S. E. Yuter, 1995: Climatological characteristics of three-dimensional storm structure from operational radar and rain gauge data. *J. Appl. Meteor.,* **34,** 1978–2007.

Stith, J. L., J. E. Dye, A. Bansemer, A. J. Heymsfield, C. A. Grainger, W. A. Petersen, and R. Cifelli, 2002: Microphysical observations of tropical clouds. *J. Appl. Meteor.,* **41,** 97–117.

Sui, C.-H., K.-M. Lau, and X. Li, 1998: Radiative–convective processes in simulated diurnal variations of tropical oceanic convection. *J. Atmos. Sci.,* **55,** 2345–2357.

Swann, H., 1998: Sensitivity to the representation of precipitating ice in CRM simulations of deep convection. *Atmos. Res.,* **47–48,** 415–435.

Tao, W.-K., and J. Simpson, 1989: Modeling study of a tropical squall-type convective line. *J. Atmos. Sci.,* **46,** 177–202.

——, and ——, 1993: The Goddard Cumulus Ensemble Model. Part I: Model description. *Terr. Atmos. Oceanic Sci.,* **4,** 19–54.

——, ——, S. Lang, M. McCumber, R. Adler, and R. Penc, 1990: An algorithm to estimate the heating budget from vertical hydrometeor profiles. *J. Appl. Meteor.,* **29,** 1232–1244.

——, ——, and S.-T. Soong, 1991: Numerical simulation of a subtropical squall line over the Taiwan Strait. *Mon. Wea. Rev.,* **119,** 2699–2723.

——, S. Lang, J. Simpson, and R. Adler, 1993: Retrieval algorithms for estimating the vertical profiles of latent heat release: Their applications for TRMM. *J. Meteor. Soc. Japan,* **71,** 685–700.

——, ——, ——, W. S. Olson, D. Johnson, B. Ferrier, C. Kummerow, and R. Adler, 2000: Retrieving vertical profiles of latent heat release in TOGA COARE convective systems using a cloud resolving model, SSM/I and radar data. *J. Meteor. Soc. Japan,* **78,** 333–355.

——, and Coauthors, 2001: Retrieved vertical profiles of latent heating release using TRMM rainfall products for February 1998. *J. Appl. Meteor.,* **40,** 957–982.

——, and Coauthors, 2003: Microphysics, radiation and surface processes in the Goddard Cumulus Ensemble (GEC) model. *Meteor. Atmos. Phys.,* **82,** 97–137.

——, J. J. Shi, S. S. Chen, S. Lang, P.-L. Lin, S.-Y. Hong, C. Peters-Lidard, and A. Hou, 2011: The impact of microphysical schemes on hurricane intensity and track. *Asia-Pac. J. Atmos. Sci.,* **47,** 1–16.

Thompson, G., R. M. Rasmussen, and K. Manning, 2004: Explicit forecasts of winter precipitation using an improved bulk microphysics scheme. Part I: Description and sensitivity analysis. *Mon. Wea. Rev.,* **132,** 519–542.

Trier, S. B., W. C. Skamarock, M. A. LeMone, and D. B. Parsons, 1996: Structure and evolution of the 22 February 1993 TOGA COARE squall line: Numerical simulations. *J. Atmos. Sci.,* **53,** 2861–2886.

Xu, K.-M., and D. A. Randall, 1996: Explicit simulation of cumulus ensembles with the GATE phase III data: Comparison with observations. *J. Atmos. Sci.,* **53,** 3710–3736.

——, and Coauthors, 2002: An intercomparison of cloud-resolving models with the Atmospheric Radiation Measurement summer 1997 intensive observation period data. *Quart. J. Roy. Meteor. Soc.,* **128,** 593–624.

Yang, S., and E. A. Smith, 1999a: Moisture budget analysis of TOGA COARE area using SSM/I retrieved latent heating and large scale Q_2 estimates. *J. Atmos. Oceanic Technol.,* **16,** 633–655.

——, and ——, 1999b: Four-dimensional structure of monthly latent heating derived from SSM/I satellite measurements. *J. Climate,* **12,** 1016–1037.

——, and ——, 2000: Vertical structure and transient behavior of convective–stratiform heating in TOGA COARE from combined satellite-sounding analysis. *J. Appl. Meteor.,* **39,** 1491–1513.

Yuter, S. E., and R. A. Houze Jr., 1995: Three-dimensional kinematic and microphysical evolution of Florida cumulonimbus. Part II: Frequency distributions of vertical velocity, reflectivity, and differential reflectivity. *Mon. Wea. Rev.,* **123,** 1941–1963.

——, ——, E. A. Smith, T. T. Wilheit, and E. Zipser, 2005: Physical characterization of tropical oceanic convection observed in KWAJEX. *J. Appl. Meteor.,* **44,** 385–415.

Zeng, X., and Coauthors, 2007: Evaluating clouds in long-term cloud-resolving model simulations with observational data. *J. Atmos. Sci.,* **64,** 4153–4177.

——, W.-K. Tao, S. Lang, A. Hou, M. Zhang, and J. Simpson, 2008: On the sensitivity of atmospheric ensembles to cloud microphysics in long-term cloud-resolving model simulations. *J. Meteor. Soc. Japan,* **86A,** 45–65.

——, and Coauthors, 2009: An indirect effect of ice nuclei on atmospheric radiation. *J. Atmos. Sci.,* **66,** 41–61.

Zhang, M. H., J. L. Lin, R. T. Cederwall, J. J. Yio, and S. C. Xie, 2001: Objective analysis of ARM IOP data: Method and sensitivity. *Mon. Wea. Rev.,* **129,** 295–311.

Zhou, Y. P., and Coauthors, 2007: Use of high-resolution satellite observations to evaluate cloud and precipitation statistics from cloud-resolving model simulations. Part I: South China Sea Monsoon Experiment. *J. Atmos. Sci.,* **64,** 4309–4329.

Zipser, E. J., D. J. Cecil, C. Liu, S. W. Nesbitt, and D. P. Yorty, 2006: Where are the most intense thunderstorms on Earth? *Bull. Amer. Meteor. Soc.,* **87,** 1057–1071.